Agent-Based Image Iris Segmentation and MultipleViews Boundary Refining

Ruggero Donida Labati, Vincenzo Piuri *Fellow, IEEE*, Fabio Scotti *Member, IEEE*

***Abstract*— The paper presents two different methods to deal with the problem of iris segmentation: an agent-based method capable to localize the center of the pupil and a method to process the iris boundaries by a multiple views approach. In the first method, an agent corresponds to the coordinates of a specific point of analysis in the input image. A population of agents is deployed in the input image, then, each agent collects local information concerning the intensity patterns visible in its region of interest. By iterations, an agent changes its position accordingly to the local properties, moving towards the estimation of the pupil center. If no available information is present in its region of interest, the agent will move itself along a random walk. After few iterations, the population tends to spread and then concentrate in the inner portion of the pupil. Once the center of the pupil has been located, the inner and outer iris boundaries are refined by an approach based on multiple views analysis. This method starts with a set of points that can be considered as an approximation of the pupil center. For each point, a detailed estimation of the iris boundaries is computed, and the final description of the iris boundaries is obtained by merging all the obtained descriptions. The two methods were tested using CASIA v.3 and UBIRIS v.2 images. Experiments show that the proposed approaches are feasible, also in eye images taken in noisy or non-ideal conditions, achieving a total error segmentation accuracy up to 97%.**

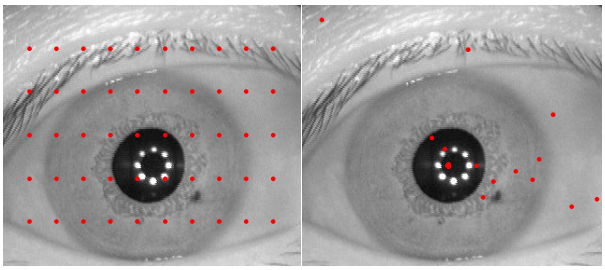

Fig. 1. Multi Agent Pupil Localization. Starting from an initial spatial configuration (left), agents search for the pupil center by an iterative approach. When the stopping criterion is reached, the area with the highest concentration of agents in the image (right) estimates the pupil center.

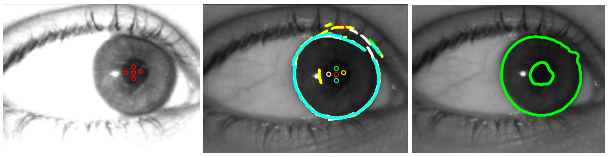

Fig. 2. Multiple Views Boundary Refining. Starting from a set of observation points inside the pupil (red circles in the left subplot), the inner and outer iris boundary are reconstructed by processing the radial gradient transitions for each observation point (colored curves in the center subplot). The different boundaries are fused in order to estimate the iris edges (right).

I. INTRODUCTION

The segmentation of the iris pattern in the input eye images is one of the most critical steps in iris biometric systems. Failures in the iris segmentation can produce relevant errors in the template creation, and hence the enroll and verification/identification procedures can be jeopardized. The research is now facing new challenges, in order to guarantee an accurate and trustworthy behavior of the system also in non ideal and noisy environments [1], [2]. The difficulty to perform reliable iris segmentation is related to the great variability associated to the aspect, position, occlusions and illumination that can be present in an eye image. Furthermore, the user cooperation, acquisition setup and environmental effect are important factors that play a decisive role in the iris segmentation, and, hence in the final behavior of the biometric systems [3], [4], [5]. In literature, the problem of the iris segmentation has been studied by different approaches. A first cluster of algorithms models the inner and outer boundaries as two circles. This category encompasses the methods where the boundaries segmentation of the iris is based on integro-differential operators [3], [6], the Hough transform [7], [8], [9], and methods based on the characteristics obtained applying *global* image operators (e.g., the Fourier transform or statistic operators) [10], [11], [12]. A second group of algorithms models the iris boundaries using a best-fit approach with *a priori* models [13], [14], or they locate the iris by analyzing *local* image features [15], [16]. Other iris segmentation methods follow hybrid/incremental approaches that initially estimate the position of the iris, and then they refine the localization/segmentation [17], [18]. The work we propose belongs to this latter category.

The contribute of the paper is twofold: we present an *agent-based* approach capable to effectively locate the center of the pupil starting with a set of candidate points displaced in the input image, then we propose a method to exploit the estimation of the pupil position and capable to identify the iris boundaries by a multiple views method. In following, we refer to the first method as Multi-Agent Pupil Localization (MAPL) and to the second method as Multiple Views Iris Boundaries Refining (MVBR).

In our previous studies [17], we demonstrated that neural networks can estimate with good accuracy the distance from the pupil center of a point in the iris with different image types. Starting from a set of points in the image, the MAPL method exploits two trained neural networks to find the pupil center position by an iterative method and a voting criterion. In MAPL, a specific point of analysis in the input image

978-1-4244-5020-6/09/$25.00 ©2009 IEEE

corresponds to the coordinates of an agent. A population of agents is deployed in the input image (Fig. 1, left subplot), then, each agent collects local information concerning the intensity patterns visible in its region of interest. By iterations, the agents change their position accordingly to the local properties, and they try to move toward the pupil center. If no available information is present in their region of interest, the agents will perform a random walk. After a few iterations, the population tends to spread and concentrate in the inner portion of the pupils (Fig. 1, right subplot). Once the termination condition is reached by the agents set, the center of the most numerous and dense cluster of agents can be effectively considered as the most probable candidate point of the pupil center.

The position of each agent near to the estimated pupil center (or the estimated center itself) can now be exploited as an observation point by MBVR (Fig. 2). Methods based on the radial gradient can produce different segmentation boundaries for different center positions, being more or less affected by occlusion and reflections. Changing the starting point of this algorithm, we change the "view point" of the iris boundaries. As a consequence, the iris boundaries, reflections and occlusions have very different shapes and positions in the linearized space obtained by different center positions. Differently, real iris boundaries tend to be more stable, even if observed by different viewpoints.

The MBVR method exploits these different behaviors in order to effectively segment the real iris boundaries. The proposed method applies in an innovative fashion the technique presented in [17], that identifies the iris boundaries by searching the peculiar pattern transitions in the radial gradient image around an observation point. In particular, we proposed to exploit a set of N observation points and then to properly fuse the extracted information in order to better interpolate the inner and outer iris boundaries. Both presented methods exploit the gray level transitions of the iris pattern, hence they can work with gray level images and color images. Furthermore, they are designed to work with different types of images. For example, the method can be applied to images acquired with specific illumination systems in controlled environments (e.g., the CASIA dataset [19]) or with noisy images with the presence of many reflections and occlusions (e.g., the UBIRIS.v2 dataset [20]).

The paper is structured as follows. Section II presents the agent-based algorithm for the search of the pupil center. Section III presents the algorithms for the search and the regularization of the iris boundaries. In Section IV, the two proposed methods are applied to different public iris image datasets, and the obtained results are then discussed and compared with state of the art methods for iris segmentation.

II. MULTI-AGENT PUPIL LOCALIZATION (MAPL)

The proposed method for the searching of the pupil center is based on a set of M agents $A(m)(m=1,\ldots,M)$, each of them characterized by the x and y coordinates in the image. Starting from an initial position, each agent computes an estimation of the pupil center coordinates and it moves itself in the estimated point. When an agent is situated far from the inner iris boundary, its movement is designed to be comparable to a random walk. When an agent is near to the real center, its movement tends to be limited or absent. When the termination criterion is reached, the final position of the pupil center is estimated observing the area of the image with the best concentration of agents. Let us detail the steps of the algorithm.

A. Initial condition of the agentes

In our implementation, the agents are distributed in the input image along a grid that regularly partitions the input eye image in a matrix of $(K+1)\times(Q+1)$ rectangles. Hence $N_A = K \times Q$ agents are displaced in the inner intersection points of the grid. In our tests, we used $K=5$ and $Q=10$. Fig. 1 plots the described initial configuration of the agents. Results indicate that the proposed method is not strongly influenced by the starting positions, a random-based initial placement of the agents can be considered as well.

B. Movementes of the agentes

In our approach, each agent is a distinct computational unit that executes the following algorithm: it collects information in its local Region of Interest (**Step B.1**); it decides the direction and the distance of the movement according to the gray level intensity transitions in the ROI (**Step B.2**); it repeats previous steps until the (collective) termination criterion is reached (**Step B.3**).

In Step B.1, the agent processes from the input image $I(x,y)$ the radial gradient image $R(x,y)$ centered in the current position $\{x_C, y_C\}$ (Fig. 3) and it extracts a circular strip image $R_p(x,y)$ centered on its current position $\{x_C, y_C\}$ inside the two radii r_{Min} and r_{Max}. Then, the delimited ROI is linearized into a rectangular image $R_p(\rho,\theta)$ by a Cartesian-Polar conversion (Fig. 3, bottom left subplot) as described in [17]. The vector $\theta = \{\theta_1, \theta_2, \ldots, \theta_M\}$ expresses the angular resolution of the analysis (typically $M = 360^o$, and $\theta_{i+1} - \theta_i = 1$). The radius r_{Max} must be fixed to a value larger than the expected iris radius in the image for the current dataset (for example $1/2$ of the minor size of the input image).

The step B.2 aims to detect in the linearized strip $R_p(\rho,\theta)$ the specific gray level transitions of the iris boundaries and then to exploit this information to estimate the proper movement of the agent $\{\Delta x, \Delta y\}$ needed to get closer to the iris center. If no estimated iris transitions are present in the linearized strip $R_p(\rho,\theta)$, the agent will perform a random jump in order to try to catch new hints of the presence of the iris pattern in a different location in the image. Fig. 4 shows the relationship existing between the shape of the iris transition (related to the observation point) and the real iris center. Let us pick a random point belonging to the pupil in the eye image (Fig. 4.a). The corresponding strip image $R_p(\rho,\theta)$ will show a quasi sinusoidal gray level transition along the θ axis, which corresponds to the pupil/iris transition (Fig. 4.b). For an ideal circular pupil, the transition is perfectly sinusoidal, and the phase and the

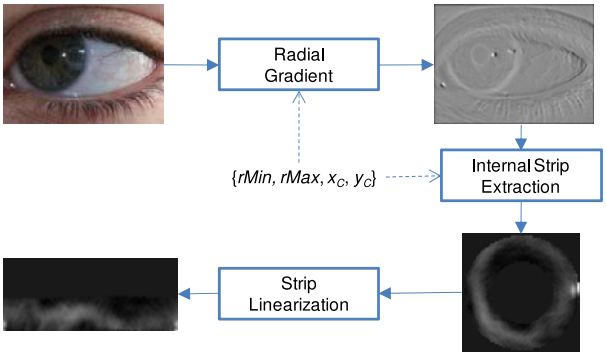

Fig. 3. Step B.1: ROI extraction. The agent extracts a linerized strip of the radial gradient image around the current position of the agent $\{x_C, y_C\}$.

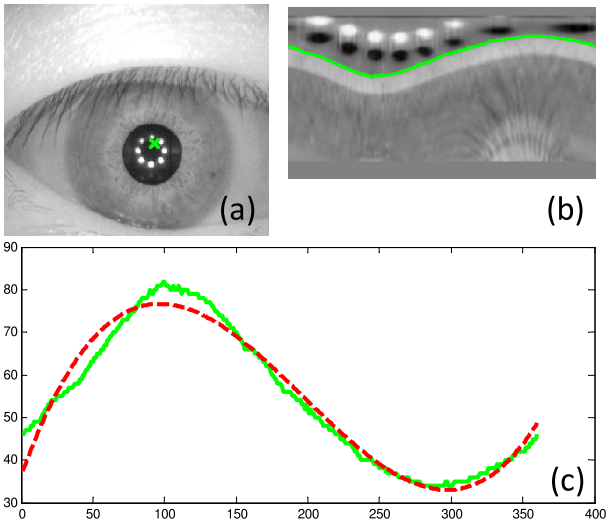

Fig. 4. Step B.2. Iris boundary detection and approximation: (a) example of observation point (central cross); (b) the related linearized strip image of the radial gradient and the estimation of the inner iris boundary $b_p(\theta)$ (green curve); (c) the third-order polynomial approximation (dashed curve) of the extracted iris boundary $b_p(\theta)$ (solid curve).

amplitude of the sinusoidal curve are directly related to the displacement of the observation point $\{\Delta x, \Delta y\}$ with respect to the real center of the pupil.

Unfortunately, in real images, the pupil is not perfectly circular, reflections and occlusions can be present and superimposed to the pupil pattern, hence the relationship between the transition pattern and the displacement $\{\Delta x, \Delta y\}$ is not trivial. In [21] we demonstrated that a feed-forward neural network can effectively learn this non linear mapping if trained with a proper set of examples. Let us now detail the method used to estimate the presence of the iris transition $b_p(\theta)$ (Fig. 4.b) in the strip image $R_p(\rho,\theta)$ and the evaluation of the agent movement $\{\Delta x, \Delta y\}$. The proposed algorithm searches the longest curve obtained from the maximum intensity columns of the bigger objects in the strip image $R_p(\rho,\theta)$ by the following steps.

B.2.1) A filtered radial gradient image $R_f(\rho,\theta)$ is processed by the radial gradient image $R_p(\rho,\theta)$ convolved with an horizontal mean filter with a $K \times 1$ kernel k_f , where

$$R_f(\rho,\theta) = R_p(\rho,\theta) * k_f.$$

B.2.2) A binarized mask $R_b(\rho,\theta)$ is created by the thresholding approach with a fixed threshold value T as follow

$$R_b(\rho,\theta) = \begin{cases} 1 & \text{if } R_f(\rho,\theta) > T \\ 0 & \text{otherwise} \end{cases}.$$

B.2.3) Within the mask $R_b(\rho,\theta)$, the N largest connected objects $\{O_1,\ldots,O_N\}$ are selected. These objects possess high radial transitions, hence they will be considered as the *candidate boundary areas*.

B.2.4) For each candidate boundary area $\{O_1(\rho,\theta),\ldots,O_N(\rho,\theta)\}$, the ρ position in each column θ with the maximum intensity value is selected, obtaining a set of candidate boundary vector $\{b_O^1(\theta),\ldots,b_O^N(\theta)\}$, where

$$b_O^i(\theta) = \underset{r_p(1-\alpha)\le\rho\le r_p(1+\alpha)}{\operatorname{argmax}} O_i(\rho,\theta).$$

B.2.5) A matrix $C(\beta,\theta)$ (where $\beta = 1\ldots N$) is created inserting the value of the radii of the candidate boundary for each θ as follows

$$C = \begin{bmatrix} b_O^1(\theta_1) & \cdots & b_O^1(\theta_M) \\ \vdots & \ddots & \vdots \\ b_O^N(\theta_1) & \cdots & b_O^N(\theta_M) \end{bmatrix}$$

The matrix $C(\beta,\theta)$ can be thought as the list for each θ of the radial positions of the boundary candidates.

B.2.6) In this step, we merge different segments belonging to the candidate boundaries in C, in order to obtain a new boundary pattern $b_p(\theta)$ (Fig. 4.b) that minimize the discontinuities. Hence, starting from the candidate objects in matrix $C(\beta,\theta)$, for each column θ of the matrix $C(\beta,\theta)$ it is extracted the radius value that is nearest to the precedent, obtaining the vector $b_p(\theta)$, where

$$b_p(\theta) = \min_{1\le\beta\le N} |C(\beta,\theta) - C(\beta,\theta-1)|.$$

B.2.7) The curve $b_p(\theta)$ is then fitted with an approximated D-order polynomial

$$\hat{Y} = w_0 + w_1 x + w_2 x^2 + \ldots + w_D x^D$$

by a linear regression function (Fig. 4.c).

B.2.8) The coefficients $W = \{w_0, w_1, \ldots, w_D\}$ are processed by two trained feed-forward neural networks in order to obtain the estimated displacement of the real pupil center as follows

$$\Delta_x = NN_x(W), \Delta_y = NN_y(W).$$

Further details on the described algorithm and the training of the neural networks are given in the result section.

C. The termination condition

In our approach we propose a termination criterion composed by two distinct conditions: the algorithm arrives to the maximum iteration number N_i (condition **TA**) or it detects a concentration of agents in a circle of radius r_B major than a fixed percentage C_A (condition **TB**). Notably, the condition TB can produce runs of the MAPL method with a different number of iterations. Moreover, it requires that each agent must control the number of other agents in its local ROI, hence producing a collective behavior about the termination condition.

D. Estimation of the pupil center

Starting from the final configuration of the agents, it is possible to estimate the position of the pupil center by searching the area of the image with the higher concentration of agents. In particular, our estimation algorithm follows the subsequent steps.

- D.1) An image $D(x,y)$ is created by counting for each pixel the number of agents that are inside a radius r_1.
- D.2) The point in $D(x,y)$ with the highest number of agents n_A is considered as the pupil center $\{x_c,y_c\}$, as follow
$$n_A = \max(D(x,y)),$$
$$\{x_c,y_c\} = \operatorname{argmax}(D(x,y)).$$
- D.3) If there are two or more points with the same value of n_A, the steps D.1 and D.2 are repeated with $r_1 = r1-1$;
- D.4) If r_1 is equal to 1 and there are two or more points with the same value of n_A, the pupil center is obtained by the mean of their coordinates.

This method can effectively manage all final agent configurations when the termination criterion is reached.

III. MULTIPLE VIEWS IRIS BOUNDARIES REFINING (MVBR)

In this section we propose a method capable to identify the iris boundaries starting from one or N points that can be considered as an approximation of pupil center (Fig. 2). Notably, these points are not necessary obtained by using the MAPL method, but they can be gathered with different methods capable to properly estimate the pupil center. In particular, the algorithm works with two input configurations:

- it is given a single observation point $P = (x_1,y_1)$ that belongs to the pupil;
- it is available an array of K observation points $P = \{(x_1,y_1),(x_2,y_2),\ldots,(x_K,y_K)\}$, where the majority of them belongs to the pupil.

This method exploits the technique presented in [17] where the boundaries of the iris are located by analyzing the pattern transition in the radial gradient image in an observation point. Differently, the MVBR method (by using in a different fashion the radial gradient image) exploits a set of N observation points, and then it fuses the extracted information in order to better interpolate the inner and outer iris boundaries. Due to the multiple view feature, the proposed method can effectively deal with reflections and occlusions. This characteristic is related to the fact that the radial gradient pattern of the reflections and occlusions is very dependent on the observation angle, for this reason, the iris boundaries description is more stable. The main steps of the proposed algorithm are the following: (**A**) the image enhancement; (**B**) in the case when only one estimated pupil center is given, $K-1$ new points are selected in the neighborhood and added to the P vector in order to better observe the iris boundaries; (**C**) for each point in P, the estimated iris boundaries are processed; (**D**) the processed boundaries are fused together in order to obtain a continuous and reliable description of the inner and outer boundary of the iris. Let us now detail the presented steps.

A. Image enhacement

This method does not need a specific image prefiltering or image enhancement. In the case of the tested datasets, only a simple histogram stretching has been used. In case, the designer can apply a specific method to enhance the iris boundary transitions, tuned with respect to the specific image type.

B. Management of the candidate obervation points P

The MVBR method produces better results if the observation points are suitably positioned around the real pupil center position. When the vector P contains only one observation point (preferably the estimated pupil center), more observation points should be added. Fig. 5 plots different configurations that can be used with a number of observation point $K = 1,3,4,5,9,13$. Differently, if a set of observation point is available, it can be directly used. For example, Fig. 5.i plots the final position of the candidate observation points obtained with the MAPL method in the corresponding image.

C. Boundaries estimation by a single obervation points

Once the observation vector P is created, the MVBR method processes the estimated inner and outer boundary of the iris for each observation point. In Step C, the procedure is very similar to the one in step B.1 of the MAPL method. In particular, the inner and the outer boundary of the iris are processed, hence two different strips (like the one plotted in Fig. 3.b) will be extracted. The minimum and maximum radii used for the inner and outer iris boundary estimation(r^i_{Min}, r^i_{Max}, R^o_{Min}, R^o_{Max}) are related to the image dataset. In this case, an enhancement Gaussian filtering was adopted for the linearized images in order to reduce the effects created by the eyelashes and by small reflections.

Given the j-th observation point in P, after this step the method processes the filtered image strips $R^j_p(\rho,\theta)$ and $R^j_i(\rho,\theta)$ of the inner and outer iris boundary, respectively. The estimation of the inner iris boundary $b^j_p(\theta)$ and of the outer iris boundary $b^j_i(\theta)$ is processed by searching the vector of pixels that has the best intensity value in every

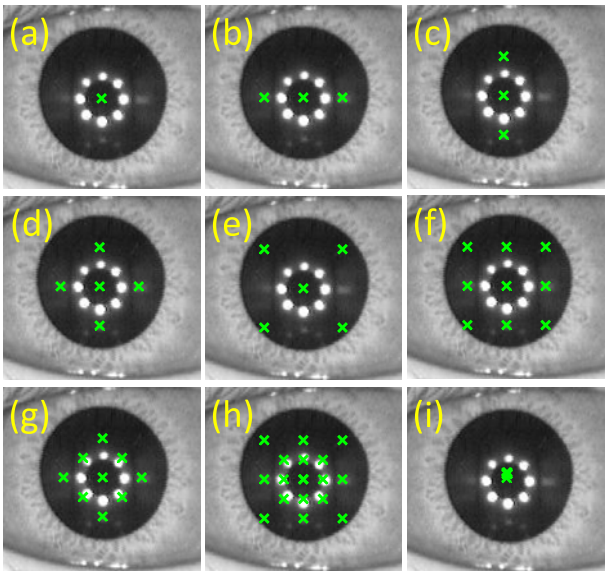

Fig. 5. Management of the candidate observation points. Starting from one single point considered as the pupil center (central point in the subplots (a)-(h)), more points can be added in different configurations to improve the behavior of the MVBR method. Subplot (i) shows a configuration of the observation points produced by using the MAPL method.

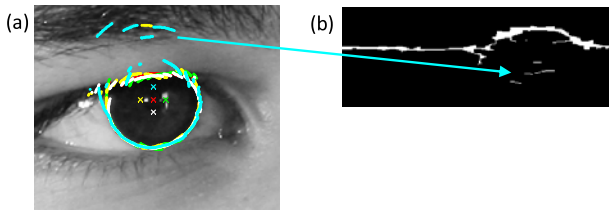

Fig. 6. Merging the multiple external boundaries. The external boundaries $B_i^j(\theta)$ (left subplot) obtained with 5 observation points (with $j = 1,\ldots,5$) are merged on a common pivot point in the polar space (right subplot). The arrow indicates the position of a candidate boundary in the Polar plane.

column of the linearized images $R_p^j(\rho,\theta)$ and $R_i^j(\rho,\theta)$, hence

$$b_p^j(\theta) = \underset{r_p(1-\alpha)\le\rho\le r_p(1+\alpha)}{\operatorname{argmax}} R_p(\rho,\theta)$$

$$b_i^j(\theta) = \underset{r_i(1-\alpha)\le\rho\le r_i(1+\alpha)}{\operatorname{argmax}} R_i(\rho,\theta)$$

D. Final boundary estimation and approximation

In Step C of the MVBR method, the inner and outer boundaries $b_p^j(\theta)$ and $b_i^j(\theta)$ have been extracted around the different K observation points in $P = \{(x_1,y_1),(x_2,y_2),\ldots,(x_K,y_K)\}$. The goal of this step is to properly merge the boundaries in a common plane. This has been done by converting all the boundaries $b_p^j(\theta)$ and $b_i^j(\theta)$ in the Cartesian space (Fig. 6.a), and then converting again all the boundaries around a common reference point (the pivot), producing the transformed boundaries $B_p^j(\theta)$ and $B_i^j(\theta)$. In this work, the pivot point is the first observation point (x_1,y_1) in P.

The outer boundaries $B_i^j(\theta)$ are plotted on a mask filled with zeros (Mask $D_i(\rho,\theta)$) as shown in Fig. 6.b The Mask $D_i(\rho,\theta)$ is processed with a morphological closure operation (with 3×3 elements), in order to obtain a more continuous curve. With a similar procedure, the inner boundaries $B_p^j(\theta)$ are used to obtain the corresponding mask $D_p(\rho,\theta)$. The information stored in the mask $D_i(\rho,\theta)$ and $D_p(\rho,\theta)$ can be now merged in order to obtain the less discontinuous inner and outer border. This procedure is equal to the MAPL steps from B.2.2 to B.2.6, where in input is given $D_i(\rho,\theta)$ and $D_p(\rho,\theta)$ and in output is obtained the regularized boundaries $e_p(\theta)$ and $e_i(\theta)$, respectively. Very often, vectors $e_p(\theta)$ and $e_i(\theta)$ can contain outliers and discontinuities; hence we propose to apply a regularization method capable to delete from the vectors the discontinuity points by the following *spike filter*. This algorithm deletes the $e_p(\theta_i)$ and $e_i(\theta_i)$ higher then a fixed threshold k_2 with respect to the mean local value in the range $\left[\theta_{i-k_2}\ldots\theta_{i+k_2}\right]$. The deleted points by the spike filter are replaced with a two-point linear interpolation between the available data. The regularized boundaries $\hat{e}_p(\theta)$ and $\hat{e}_i(\theta)$ are hence converted in the Cartesian space.

IV. EXPERIMENTAL RESULTS

In this section we present the results obtained by MAPL and MVBR methods on different datasets. The first dataset (**Dataset A**) is composed by 100 images randomly selected from the CASIA-IrisV3-Interval database [16]. For dataset A, a trained supervisor selected the centers of the pupils in all images, producing the reference for the pupils centers as suggested in [20]. At best of our knowledge, no such direct comparisons are available in the liteature. The second dataset (**Dataset B**) is composed by 20 images randomly selected from the Dataset A. The third (**Dataset C**) is composed by all the images of UBIRIS.v2 [21] with the iris not completely occluded (477 images). For all images of Dataset B and Dataset C, a supervisor produced a manual segmentation of each pixel belonging to the iris pixel, producing the references to process the segmentation error of the algorithm. The parameters of MAPL method have been empirically tuned for the CASIA image type, obtaining $r_{Min} = 2$ pixel, $r_{Max} = 50$ pixel, $N = 7$ objects, $T = 10\%$ of the maximum intensity of each linearized strip. The configuration of the neural networks is with a single input layer composed by two log-sigmoid layers with 12 and 5 neurons respectively, trained with the back-propagation algorithm [20]. The number of the agents in the first iteration is 50 (their position can be described by a 5×10 equally spaced grid).

We tested the MAPL method on Dataset A with the two termination criteria. Fig. 7 plots the results obtained with the termination criterion TA. For each iteration, it is plotted the number of images that obtained a position of the estimated center with an Euclidean distance less than 2, 3, 5, 10 pixels to the reference pupil center, in the different iterations. The results show that the agents converge with good accuracy in the pupil center after a few iterations. Fig. 8 plots the results obtained with the termination criterion B, showing the percentage of images with the pupil center estimated with an error minor of 2,3,5,10 pixels with respect to the concentration of agents in the center. Results show that

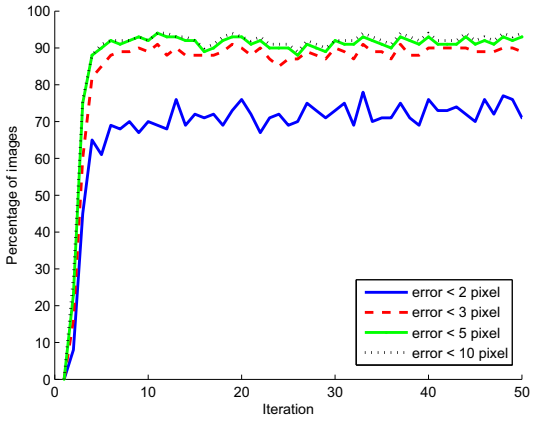

Fig. 7. Percentage of images with the pupil center estimated with an error minor of 2,3,5,10 pixels with respect to the iteration number of the MAPL algorithm on the Dataset A (Termination Criterion TA).

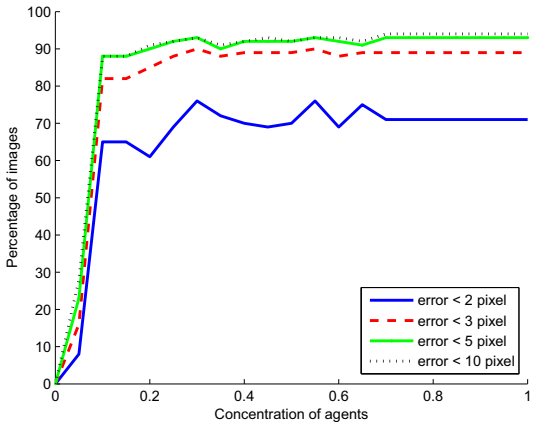

Fig. 8. Percentage of images with the pupil center estimated with an error minor of 2,3,5,10 pixels with respect to the parameter Concentration of Agents C_A with $r_B = 3$ pixels on Dataset A (Termination Criterion TB).

even a small concentration of agents in a point can suitably estimate the presence of the pupil, hence the early-stopping criterion is effective and it produces a better accuracy than the single condition TA. In addition, it strongly reduces the number of iterations made by the agents

The overall behavior of MAPL method is sufficient since the pupil has been located with an error less than 5 pixels for the 93% of the images in Dataset A.

We compared also the proposed algorithm to different techniques available in the literature for locating the iris center: a public code library based on based on the Hough operator [22] (**Method A**) and the algorithm presented in [3] (**Method B**). For the 94% of the images of Dataset A, the pupil center estimation computed by MAPL method is more accurate than the result obtained by Method A, and for the 93% of this images, MAPL is more accurate than Method B. The MAPL method has an elevated computational complexity and it cannot work in real-time applications: the computation of each image requires 15 minutes on an Intel Core2 Duo 2.4GHz working with Windows XP. All presented algorithms have been written in Matlab language (Version 7.6) exploiting the available toolboxes.

TABLE I

ACCURACY OF THE MVBR SEGMENTATION ON DATASET B.

Config.	TP (%)	TN (%)	FP (%)	FN (%)	Sensitivity (%)	Specificity (%)	Total Error (%)
A	23.771	66.336	8.6973	1.1956	95.2210	88.4088	9.8930
B	23.031	67.352	7.6820	1.9359	92.2461	89.7619	9.6179
C	23.051	67.409	7.6247	1.9158	92.3265	89.8382	9.5405
D	23.442	69.250	5.7834	1.5245	93.8938	92.2923	7.3079
E	23.445	69.453	5.5804	1.5213	93.9068	92.5628	7.1016
F	23.247	71.651	3.3824	1.7198	93.1117	95.4921	5.1022
G	23.637	70.556	4.4776	1.3292	94.6759	94.0326	5.8068
H	23.540	71.833	3.2003	1.4265	94.2865	95.7349	4.6267
I	23.648	67.488	7.5456	0.3184	98.7246	89.9436	7.8641

Note: Percentage of iris pixel =24.967% (Positive case);
TP=True Positive; TN=True Negative; FP=False Positive; FN=False Negative.

The parameters of the MVBR have been tuned to the following values for the Dataset B: $r^i_{Min} = 15$ pixel, $r^i_{Max} = 90$ pixel, $k_1 = 4$ pixel, $k_2 = 0.5$, and no Gaussian filter for the inner iris boundary detection; $r^o_{Min} = 90$ pixel, $r^o_{Max} = 130$ pixel, $k_1 = 20$ pixel, $k_2 = 1.5$, and a $[10 \times 30]$ Gaussian kernel with $\sigma = 30$ for the outer iris boundary detection. For Dataset C the parameters are: $r^i_{Min} = 2$ pixel, $r^i_{Max} = 35$ pixel, $k_1 = 20$ pixel, $k_2 = 0.5$, and a $[20 \times 20]$ Gaussian kernel with $\sigma = 10$ for the inner iris boundary detection; $r^o_{Min} = 30$ pixel, $r^o_{Max} = 90$ pixel, $k_1 = 20$ pixel, $k_2 = 2$, and a $[5 \times 30]$ Gaussian kernel with $\sigma = 30$ for the outer iris boundary detection. The quantitative tests of the MVBR method were performed with Dataset B and Dataset C by a pixel-by-pixel comparison with the supervised reference masks of the iris pattern (Fig. 8.a-d show examples of the reference masks). The test performed with Dataset B compared 1792000 pixels with an error rate of 4.6%. The complete results are given in Table I, where the different configurations shown in Fig. 5 are compared. The candidate observation points are obtained by the results of the MAPL method for Dataset B, and with a set of manually selected points for Dataset C. Results show that the accuracy of the MAPL+MVBR method (Table I) is correlated by the number of observation points. In fact, the minor total error was obtained by the configuration H. The configuration I is composed by an elevate number of agents, but it does not offer a good accuracy because the candidate observation points are too concentrated in a small area around the pupil center.

The MVBR results on Dataset C are given in Table II, where where the best total segmentation error is equal to 2.9%. This value was obtained with the protocol of the competition [21] using the same image dataset. Notably, the errors obtained by the 8 best methods ranked in the international competition range from 1.3% and 3.05% , where five of them are in the 2-3% range. Particularly, the results of this work were obtained without any eyelashes location and reflections removal methods. Fig. 9 shows the application of the MVBR method on two example images taken from Dataset B (9.a and 9.b) and on two example images taken from Dataset C (9.c and 9.d). A qualitative analysis shows a correct behavior of the MVBR method while it correctly follows the iris

TABLE II

ACCURACY OF THE MVBR SEGMENTATION ON DATASET C.

Config.	TP (%)	TN (%)	FP (%)	FN (%)	Sensitivity (%)	Specificity (%)	Total Error (%)
A	6.278	90.102	2.6583	0.9614	86.7193	97.1342	3.6198
B	6.385	90.461	2.2996	0.8544	88.1983	97.5209	3.1540
C	6.372	90.518	2.2422	0.8671	88.0231	97.5828	3.1092
D	6.362	90.610	2.1506	0.8771	87.8847	97.6816	3.0277
E	6.423	90.642	2.1186	0.8161	88.7264	97.7161	2.9347
F	6.422	90.656	2.1047	0.8179	88.7026	97.7311	2.9225
G	6.341	90.610	2.1509	0.8982	87.5929	97.6813	3.0491
H	6.425	90.650	2.1102	0.8149	88.7429	97.7251	2.9252

Note: Percentage of iris pixel =7.239% (Positive case);

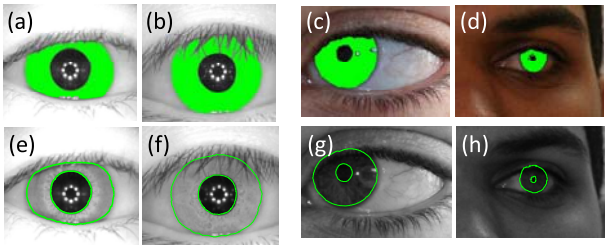

Fig. 9. Examples of a segmented image by the supervisor (a-d), and the boundaries $\hat{e}_p(\theta)$ and $\hat{e}_i(\theta)$ obtained by the MVBR method (e-h).

boundaries in very different image types.

The computational time required for the estimation of the iris boundaries depends on the number of the used observation points. Approximately, 0.68 second is required for each observation point on an Intel Core2 Duo 2.4GHz working with Windows XP.

V. CONCLUSIONS

The paper presented an agent-based method to locate the center of the pupil in an eye image and a method capable to find and refine the inner and outer boundary of the iris, based on multiple views observations. Experimental results showed that the methods can effectively work with different dataset types, also with images taken in noisy and non-ideal conditions. Future work are needed to extend the applicability of the methods by automatically tune the methods' parameters to the current test dataset and including algorithms for the eyelashes removal.

VI. ACKNOWLEDGEMENTS

This research has been partially funded by the European Communitys Seventh Framework Programme (FP7/2007-2013) under grant agreement no. 216483, and by the Italian Ministry of Education, University and Research under the grant no. PRIN 2007JXH7ET.

REFERENCES

[1] J. R. Matey, R. Broussard, and L. Kennell, "Iris image segmentation and sub-optimal images," *Image and Vision Computing*, vol. In Press, 2009.

[2] H. Proenca and L. Alexandre, "Iris segmentation methodology for non-cooperative recognition," *Vision, Image and Signal Processing, IEEE Proceedings* -, vol. 153, no. 2, pp. 199–205, April 2006.

[3] J. Daugman, "How iris recognition works," in *Image Processing. 2002. Proceedings. 2002 International Conference on*, vol. 1, 2002, pp. 33–36.

[4] W. Boles and B. Boashash, "A human identification technique using images of the iris and wavelet transform," *Signal Processing, IEEE Transactions on*, vol. 46, no. 4, pp. 1185–1188, Apr 1998.

[5] C. Fancourt, L. Bogoni, K. Hanna, Y. Guo, R. Wildes, N. Takahashi, and U. Jain, "Iris recognition at a distance," in *Audio and Video Based Biometric Person Authentication*. Springer Berlin / Heidelberg, 2005, vol. 3546, pp. 1–13.

[6] J. Zuo, N. Kalka, and N. Schmid, "A robust iris segmentation procedure for unconstrained subject presentation," in *Biometric Consortium Conference, 2006 Biometrics Symposium: Special Session on Research at the*, Aug. 2006, pp. 1–6.

[7] R. Wildes, "Iris recognition: an emerging biometric technology," *Proceedings of the IEEE*, vol. 85, no. 9, pp. 1348–1363, Sep 1997.

[8] X. Liu, K. Bowyer, and P. Flynn, "Experiments with an improved iris segmentation algorithm," in *Automatic Identification Advanced Technologies, 2005. Fourth IEEE Workshop on*, Oct. 2005, pp. 118–123.

[9] X. He and P. Shi, "A new segmentation approach for iris recognition based on hand-held capture device," *Pattern Recogn.*, vol. 40, no. 4, pp. 1326–1333, 2007.

[10] N. Puhan, N. Sudha, and X. Jiang, "Robust eyeball segmentation in noisy iris images using fourier spectral density," in *Information, Communications and Signal Processing, 2007 6th International Conference on*, Dec. 2007, pp. 1–5.

[11] L. Kennell, R. Ives, and R. Gaunt, "Binary morphology and local statistics applied to iris segmentation for recognition," in *Image Processing, 2006 IEEE International Conference on*, Oct. 2006, pp. 293–296.

[12] R. Ives, L. Kennell, R. Gaunt, and D. Etter, "Iris segmentation for recognition using local statistics," in *Signals, Systems and Computers, 2005. Conference Record of the Thirty-Ninth Asilomar Conference on*, November 2005, pp. 859–863.

[13] G. Xu, Z. Zhang, and Y. Ma, "Improving the performance of iris recogniton system using eyelids and eyelashes detection and iris image enhancement," in *Cognitive Informatics, 2006. ICCI 2006. 5th IEEE International Conference on*, vol. 2, July 2006, pp. 871–876.

[14] J. Daugman, "New methods in iris recognition," *Systems, Man, and Cybernetics, Part B: Cybernetics, IEEE Transactions on*, vol. 37, no. 5, pp. 1167–1175, Oct. 2007.

[15] A. Ross and S. Shah, "Segmenting non-ideal irises using geodesic active contours," in *Biometric Consortium Conference, 2006 Biometrics Symposium: Special Session on Research at the*, Aug. 2006, pp. 1–6.

[16] C.B.S.R., Center for Biometrics and Security Research, http://www.cbsr.ia.ac.cn.

[17] R. Donida Labati and F. Scotti, "Noisy iris segmentation with boundary regularization and reflections removal," *Image and Vision Computing*, vol. In Press.

[18] R. Broussard, L. Kennell, D. Soldan, and R. Ives, "Using artificial neural networks and feature saliency techniques for improved iris segmentation," in *Neural Networks, 2007. IJCNN 2007. International Joint Conference on*, Aug. 2007, pp. 1283–1288.

[19] H. Proena, S. Filipe, R. Santos, J. Oliveira, and L. A. Alexandre, "The ubiris.v2: A database of visible wavelength images captured on-the-move and at-a-distance," *IEEE Transactions on Pattern Analysis and Machine Intelligence*, vol. In Press.

[20] R. Donida Labati, V. Piuri, and F. Scotti, "Neural-based iterative approach for iris detection in iris recognition systems," in *IEEE Symposium: Computational Intelligence for Security and Defence Applications (CISDA), 2009*, vol. In Press.

[21] H. Proenca and L. Alexandre, "The NICE.I: Noisy Iris Challenge Evaluation - Part I," in *Biometrics: Theory, Applications, and Systems, 2007. BTAS 2007. First IEEE International Conference on*, Sept. 2007, pp. 1–4.

[22] L. Masek and P. Kovesi, *MATLAB Source Code for a Biometric Identification System Based on Iris Patterns*. The School of Computer Science and Software Engineering, The University of Western Australia, 2003.